Fatigue Failure Investigation - Putnam Bridge

John T. DeWolf

Kevin J. Bernard,
Graduate Assistant

December 1994

JHR 94-237 **Project 92-2**

This research was sponsored by the Joint Highway Research Advisory Council (JHRAC) of the University of Connecticut and the Connecticut Department of Transportation and was carried out in the Civil Engineering Department of the University of Connecticut.

Technical Report Documentation Page

1. Report No.	2. Government Accession No.	3. Recipient's Catalog No.
JHR 94-237		

4. Title and Subtitle	5. Report Date
Fatigue Failure Investigation - Putnam Bridge	December 1994
	6. Performing Organization Code
7. Author(s)	8. Performing Orgonization Report No.
John T. DeWolf and Kevin J. Bernard	JHR 94-237
9. Performing Organization Name and Address	10. Work Unit No. (TRAIS)
University of Connecticut Department of Civil Engineering 191 Auditorium Road, Box U-37 TI Storrs, CT 06269	11. Contract or Grant No.
	13. Type of Report and Period Covered
12. Sponsoring Agency Name and Address	Final Report
Connecticut Department of Transportation 280 West Street Rocky Hill, CT 06067-0207	14. Sponsoring Agency Code

15. Supplementary Notes

16. Abstract

The Putnam Bridge, which spans the Connecticut River in Glastonbury Connecticut, has experienced fatigue failures in the transverse beam connections which are near the supports. The A325 bolts are failing in tension, and cracks are developing in the connected parts. The bridge was monitored using a portable computer-based strain gage data acquisition system. Live load stress data were collected at different locations. Results were also compared with finite element analyses to further define how loading affects these connections. The cause of the fatigue problem was determined. AASHTO bridge fatigue guidelines have been used to give long-term performance predictions. Recommendations are given on repair.

17. Key Words	18. Distribution Statement
Bridge monitoring, strain monitoring, fatigue, bolted connections	No Restrictions

19. Security Classif. (of this report)	20. Security Classif. (of this page)	21. No. of Pages	22. Price
Unclassified	Unclassified	35	

Form DOT F 1700.7 (8-72) Reproduction of completed page authorized

ACKNOWLEDGEMENTS

This report is adapted from the M.S. thesis submitted by Kevin Bernard, Graduate Assistant.

This work could not have been completed without the assistance of ConnDOT and in particular Mr. Michael Culmo of the Connecticut Department of Transportation Bridge Design Unit.

Mr. Richard Sartor, graduate assistant at the University of Connecticut, provided assistance during the configuration and calibration of the system and during the collection of the field data.

SI* (MODERN METRIC) CONVERSION FACTORS

APPROXIMATE CONVERSIONS TO SI UNITS

Symbol	When You Know	Multiply By	To Find	Symbol
LENGTH				
in	inches	25.4	millimetres	mm
ft	feet	0.305	metres	m
yd	yards	0.914	metres	m
mi	miles	1.61	kilometres	km
AREA				
in^2	square inches	645.2	millimetres squared	mm^2
ft^2	square feet	0.093	metres squared	m^2
yd^2	square yards	0.836	metres squared	m^2
ac	acres	0.405	hectares	ha
mi^2	square miles	2.59	kilometres squared	km^2
VOLUME				
fl oz	fluid ounces	29.57	millilitres	mL
gal	gallons	3.785	Litres	L
ft^3	cubic feet	0.028	metres cubed	m^3
yd^3	cubic yards	0.765	metres cubed	m^3
NOTE: Volumes greator than 1000 L shall be shown in m^3.				
MASS				
oz	ounces	28.35	grams	g
lb	pounds	0.454	kilograms	kg
T	short tons (2000 lb)	0.907	megagrams	Mg
TEMPERATURE (exact)				
°F	Fahrenheit temperature	5(F-32)/9	Celcius temperature	°C

*SI is the symbol for the International System of Measurement

APPROXIMATE CONVERSIONS TO SI UNITS

Symbol	When You Know	Multiply By	To Find	Symbol
LENGTH				
mm	millimetres	0.039	inches	in
m	metres	3.28	feet	ft
m	metres	1.09	yards	yd
km	kilometres	0.621	miles	mi
AREA				
mm^2	millimetres squared	0.0016	square inches	in^2
m^2	metres squared	10.764	square feet	ft^2
ha	hectares	2.47	acres	ac
km^2	kilometres squared	0.386	square miles	mi^2
VOLUME				
mL	millilitres	0.034	fluid ounces	fl oz
L	litres	0.264	gallons	gal
m^3	metres cubed	35.315	cubic feet	ft^3
m^3	metres cubed	1.308	cubic yards	yd^3
MASS				
g	grams	0.035	ounces	oz
kg	kilograms	2.205	pounds	lb
Mg	megagrams	1.102	short tons (2000 lb)	T
TEMPERATURE (exact)				
°C	Celcius temperature	1.8C + 32	Fahrenheit temperature	°F

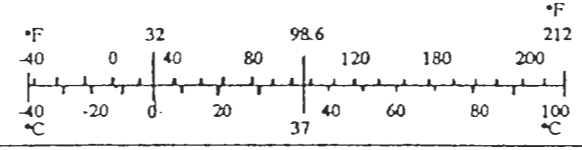

TABLE OF CONTENTS

LIST OF FIGURES

LIST OF TABLES

CHAPTER 1

BACKGROUND AND OBJECTIVES

According to the Federal Highway Administration's report to Congress, as of June 1988, 23.5 percent of 577,710 United States' highway bridges are classified as structurally deficient and 17.7 percent are functionally obsolete (Dunker and Rubbal). A majority of these bridges with fatigue cracking problems are those that are reaching their 35 to 50 year service life. The causes of these problems have been attributed to increases in the allowable truck weights, an increase in heavy truck traffic, and deformations which were not anticipated in the original design.

The current provisions in the American Association of State Highway and Transportation Officials (AASHTO) Guide Specifications for Fatigue Evaluation of Existing Steel Bridges and the AASHTO Bridge Design Manual 14th edition have requirements for fatigue evaluation and design of steel bridge members. The Fatigue Evaluation Guide recommends collecting in-service live load stress histograms. One of the most reliable methods of determining actual live load stresses in the field is to utilize portable strain gage data acquisition equipment. The Putnam Bridge was investigated with a new system, developed for this project.

CHAPTER 2

BEHAVIOR AND FIELD TESTS

DESCRIPTION OF BRIDGE

The Putnam Bridge was designed in 1957 and completed in December 1958. It is a four-lane, symmetrical, nonredundant bridge with two travel lanes in each direction. It consists of 14 spans, comprised of nine 120 foot, simply supported approach spans at each end, and longer continuous spans which cross the Connecticut River. Problems occurring in the simple spans are treated in this report.

Each simply supported span is composed of two main riveted, noncomposite longitudinal girders that support five evenly spaced, riveted transverse floor beams that are composite with the concrete deck slab. In turn, these transverse floor beams receive the end reactions of longitudinal W24x76 rolled sections that are also composite with the deck slab (see Figures 2.1 & 2.2). These girders and beams are made of low alloy steel.

This investigation was conducted at the first 120 foot southerly span, due to its accessibility from the ground. This span is representative of the other nine simply supported spans which are experiencing similar cracking problems.

Fatigue cracking of the connection angles and bolts occurs at the top of the cantilever arm of the transverse beam which is connected to the longitudinal girders (see Figure 2.3).

GENERAL BEHAVIOR

Fisher (Fisher, Yen, Daniels) looked at fatigue cracking due to differential displacements in the Lehigh Canal Bridge in Pennsylvania. Figure 2.4 shows a cross section of the Lehigh Canal Bridge at the connection between the longitudinal girder and transverse beam. This bridge is similar in design to the Putnam Bridge. Fisher concluded that a differential displacement of the longitudinal girder's top flange, with respect to the transverse beam's top flange, caused fatigue cracking of connection plates. Figure 2.5 shows how the composite transverse beam and longitudinal girder should be connected to avoid problems. Since all three components are composite with the concrete deck slab, no fatigue problems occur in the connection detail with this type of integrated framing system.

In the Putnam Bridge, angles were used instead of connection plates for the detail under examination and only the transverse beam bears against the top slab and is composite (see Figure 2.3). Thus, the relative displacements between the longitudinal and

transverse girders, due to the horizontal displacement under live load, are thought to be non-compatible (see Figure 2.3).

As of May 1993, fatigue cracking of the angles had occurred at one location and failure of the A325 7/8" diameter bolts had occurred at eight locations in the test span. A visual investigation of the failed bolts showed no signs of bearing or bending. It was assumed that the bolts failed due to fatigue loading in prying tension and the bolt's failure followed the three characteristic regions of fatigue failure as Fisher states:

> The first region corresponds to slow stable crack growth. This has a visually smooth surface. The second region is rougher in texture as the distance and rate of growth from the nucleus of the fatigue crack increases. The third region is the final fracture, which may be either brittle or ductile, depending on the circumstances. (Kulak, Fisher, Struik)

No failures occurred at the span's center-line connection and only two failures occurred at the connection nearest the centerline, while four failures were recorded at the span's ends. It was assumed that the key factor is the amount of rotation occurring in the longitudinal beam under live loading. There is minimal rotation near the center, with maximum rotation occurring at the bridge ends. As shown in Figure 2.6, this live load rotation causes a longitudinal displacement of the top flange of the girder. This displacement is a product of the slope at the end and the distance from the neutral axis of the longitudinal girder. One may consider the connection similar to a shear connector between the concrete deck and the longitudinal girders, and also consider the behavior similar to a Vierendeel truss which resists load by developing bending moments at its joints. Both types of behavior were not anticipated.

Looking specifically at the angle connection, bolt failures occurred almost entirely in the bottom bolt row (see Figure 2.7). This stress pattern indicates a prying action caused by the longitudinal displacement of the girder. This prying action begins at the base of the connection and decreases toward the top of the connection.

This behavior is similar to a fixed-fixed column with an induced lateral displacement. The angle base and the first row of bolts form the fixed-ended supports. This is demonstrated in Figure 2.8. Since the angle pivots around the lower row of bolts, as the displacement occurs under girder rotation, the top row of bolts loses tension. This explains why the bolts in the top row of the connection are not failing.

RETROFIT MODIFICATION AND REPAIR

Based upon the results of the Connecticut Department of Transportation bridge inspection reports outlining the angle and bolt failures, modification of the connection angle was carried out as shown in Figure 2.9. A pair of 4" x 8" x 1/2" plates were welded to each angle leg. This modification was made on March 26, 1990 to stiffen the failing angle. It also served to repair the cracked angle by making it continuous with the welds along the added stiffener plates. It was determined that by increasing the angle stiffness, the distortions which caused the fatigue problems would be minimized. However, a ConnDOT bridge inspection report dated October 9, 1991, noted that the intended repairs had failed within a year and a half.

FIELD TESTS

Field tests were used to explore in detail the continued cracking and to verify assumptions made on the behavior.

Strain gages and strain gaged bolts were used to record the live load stresses of random, daily, afternoon traffic. These sensors were placed at the connection angles and at the longitudinal girder's center line flanges.

New A325, 7/8" diameter bolts were installed at the abutment, quarter point and center line angle connections by a ConnDOT bridge maintenance crew. These bolts were modified with two strain gages welded to them, one on either side. The gaged bolts were orientated in the connection so that the gages lay on a horizontal plane (i.e. the neutral axis of the bending cross section). This minimized the measurement of any bolt tensile prying action. The strains from these two gages were averaged, in order to determine the tensile force occurring under live load.

One strain gage was installed on the north side of the abutment connection angle. The abutment backwall prevented the installation of a strain gage on the opposite side of this connection angle. One strain gage was installed on each side of the quarter point angle connection. Figure 2.7 shows the locations of the gaged bolts and strain gages at points A, B and C.

Strain gages were also placed on the top and bottom flanges of the longitudinal girder at its center line location. These were used to measure the bending stress in the girder and to determine its neutral axis location. The gage at the center line of the bottom flange of the longitudinal girder was used as the trigger to start the computerized stress recording of the live load event. It was set at 0.3 ksi, equivalent approximately to the live load stress for the lightest truck observed during the preliminary sampling run.

As shown in Figure 2.10, the bottom flange bending stress is approximately 30 percent greater than the top flange bending stress. The longitudinal girder is non-prismatic, with a symmetrical cross section. Since the neutral axis does not lie at the girder's center line, but is 8.7 inches above it, partial composite action is developed, due to the concrete deck slab which is connected at the quarter points to the longitudinal girder. This composite force is transferred primarily by the angle connections acting as shear connectors and by the transverse beam's web that is connected to the longitudinal girder. This was not anticipated in the original design.

Although no vehicles were weighed, visual observation of the random traffic loading showed that, what appeared to be a typically loaded 5-axle tractor trailer truck, (Type 3-S2), caused approximately a 13 ksi bending stress at the gage location (26.9 ksi at base) on the abutment angle. This corresponds to a 0.9 ksi stress in the longitudinal girder's bottom flange. One truck induced a 36 ksi stress reading at the abutment angle gage location. This truck was carrying a large excavator. The corresponding stress in the longitudinal girder's bottom flange was 3.2 ksi (see Figure 2.11). Table 2.12 shows the average stresses at angle base locations caused by particular vehicle types.

Figure 2.12 shows a typical, four-minute stress monitoring of the longitudinal girder and abutment angle under random, daily, afternoon traffic. Figure 2.13 shows an enlarged section of Figure 2.12 between 2 minutes and 2 minutes 30 seconds. Note that the abutment angle undergoes a stress reversal as the longitudinal girder's bottom flange displays a negative stress. This negative

	ABUTMENT ANGLE (BASE)	QUARTER POINT ANGLE (NORTH SIDE)	LONGITUDINAL GIRDER (CENTER LINE)
Automobile:	5.4 ksi	3.7 ksi	0.18 ksi
2 Axle Truck: (Type 3)	17.4	13.2	0.6
5 Axle Truck: (Type 3-S2)	26.9	19.7	0.9 (3.2 Peak)

Table 2.12

AVERAGE STRESS AT ANGLE vs VEHICLE TYPE

stress indicates upward bending of the longitudinal girder, caused by a heavy truck traveling in the other direction over the opposite longitudinal girder. As can be seen in Fig. 2.13, the abutment angle undergoes a 5 ksi stress range at the angle location, resulting in approximately a 10.0 ksi stress range at the angle base. Therefore truck traffic in the opposite lane also induces a large stress range with reversal on the connection angles. This also was not anticipated in the design considerations for this bridge.

CHAPTER 3

ANALYSIS OF FIELD TEST DATA

Using the AASHTO Fatigue Evaluation Specification, the effective stress range for the abutment, quarter point and center line angles was calculated and compared to the AASHTO allowable values.

Since a strain gage could not be attached to the base of the angle due to physical constraints, a linear interpolation of the stress at the base was performed knowing the angle dimensions, gage location and the measured stress. This is a reasonable approach, since the moment diagram, due to the transverse displacement, and thus, the stress diagram, is linear (see Figure 2.8).

The effective stress range was determined using the AASHTO Effective Stress Range formula (Miner's Rule). The formula states:

$$S_r = [\sum f_i S_{ri}^3]^{0.33}$$

where:

S_r = the effective stress range.
f_i = fraction of stress ranges within an interval.
S_{ri} = midwidth of the interval.

Using this equation, the effective stress range at the gage location on the abutment angle was 12.85 ksi. Using linear interpolation, the effective stress range at the base of the abutment angle is then 27.3 ksi. The quarter point had an effective stress range of 22.7 ksi at the base of the angle, and the center line point equalled 1.8 ksi. The AASHTO Fatigue Guide recommends that the maximum stress range for an infinite fatigue life (S_{FL}) is 8.8 ksi for this Fatigue Detail Category A. Therefore, only the center line connection should last indefinitely.

According to the 1991 ConnDOT Average Daily Truck Traffic (ADTT) Survey for Urban Arteries, heavy vehicles averaged 4.02% of all state-wide vehicle traffic. The total traffic count of all vehicle types crossing the Putnam Bridge in 1990 is 20,800 Eastbound and 19,900 Westbound (gaged direction) per day. Assuming these figures are accurate and have not changed drastically, approximately 800 trucks per day cross the bridge over the gaged longitudinal girder. Using this data and the AASHTO Fatigue Guide, the Finite Remaining Life (Y_f) of the angle at the abutment and quarter point were calculated. The Finite Remaining Life equation is:

$$Y_f = \left[\frac{f\,K \cdot 10^6}{T\,C\,(R\,S_r)^3}\right] - a$$

where:

Y_f = remaining fatigue life in years.
K = detail constant; equal to 68 for this detail, Category A.
T = estimated lifetime average daily truck volume assuming a 4% yearly increase.
C = stress cycles per truck passage; equals 1.0 for one stress cycle per truck passage (simple span).
S_r = effective stress range.
R = reliability factor; equals 1.35 for redundant members.
a = present age of the bridge in years; equals 34 years.
f = 1.0 for calculating safe life.

Based on consultations with ConnDOT engineers on the current yearly increase in truck traffic, a 4% inflation rate in truck traffic was assumed.

The two coefficients of this formula that have a large influence on the final result are: the effective stress range value (S_r) and the lifetime average daily truck traffic volume (T). The effective stress range was determined from the field data, under what appeared to be typical daily truck traffic. This is the most sensitive of the two coefficients, since a slight change in this value results in a geometric change in remaining life. The remaining controlling factor, the average daily truck traffic, was based on the ConnDOT ADTT reports and the two days of data collection.

Table 3.1 shows the effective stress range and remaining life values for the abutment, quarter and center line connections at the angle base.

	Fatigue Location		
	Abutment	Quarter	Center
S_r:	27.3 ksi	22.7 ksi	1.8 ksi
Y_f:	-32 years	-29 years	N/A, (S_r<S_{FL})

TABLE 3.1

EFFECTIVE STRESS RANGE vs FINITE REMAINING FATIGUE LIFE

From Table 3.1, the abutment and the quarter point are either well out of range for this approach or have no finite life

remaining due to their high effective stress ranges. The center line point appears to have an infinite fatigue life since its stress range of 1.8 ksi is well below the AASHTO infinite fatigue life limit of 8.8 ksi. These are reasonable expectations, since the investigated abutment and quarter point angles show signs of fatigue induced cracking of the surface paint in the same location as a number of the abutment angles that have already failed. Also, since the gaged abutment angle was one that was recently replaced, it is expected that this angle also will fail in a short time.

BOLT STRESSES

Figure 3.1 shows the stresses for the strain gaged bolts at the abutment (bottom row), quarter point and center line angle connections under random, daily, afternoon traffic. Table 3.2 shows the typical peak stresses obtained in the gaged abutment (bottom), quarter point and center line bolts. These results show that the bolt stresses are much lower than the 27.5 ksi that AASHTO allows for fatigue tensile loading of A325 bolts. There are, however, many bolts failing at these angle connection details.

According to the Proposed Revisions to the AASHTO Standard Specifications for Structural Supports for Highway Signs, Luminaries, and Traffic Signals, these bolts will be in Fatigue Detail Category E with an allowable stress range of 4.5 ksi. This allowable stress range is still greater than the stress results obtained by the gaged bolts on the bridge.

Since the gaged bolts were installed with the strain gages in the plane of the neutral axis and at the mid-length of the bolt, tensile stresses from any localized bending of the bolt under prying action of the displaced angle were not measured. It is thus felt that the localized bending, due to this prying force on the bolt, occurring at the base of the nut, combined with the direct tensile force, is the cause of bolt failures. The failure occurs where stress concentrations exist, due to the thread grooves.

	ABUTMENT BOLT	QUARTER POINT BOLT	CENTER LINE BOLT
Automobile:	0.5 ksi	0.3 ksi	0.02 ksi
2 Axle Truck: (Type 2)	2.6	2.1	0.05
5 Axle Truck: (Type 3-S2)	4.1	3.4	0.08

TABLE 3.2

AVERAGE GAGED BOLT STRESS vs VEHICLE TYPE

CHAPTER 4

ANALYTICAL STUDY

GLOBAL BRIDGE MODEL

A finite element model of the entire 120 foot span was created. Since fatigue cracking may be the result of a 1/1000 of an inch distortion and also be the result of three dimensional behavior, a finite element model will not accurately predict specific fatigue problems. The model was used however to determine the relative displacements and rotations between the concrete slab, transverse floor beams and the longitudinal girders. A correlation, between the location of the failed connections and the amount of displacement, can be deduced and correlated with the field stress measurements.

Following the bridge modeling recommendations (Jategaonkar, Jaeger and Cheung), a finite element mesh was generated at the slab's mid-depth (see Figure 4.1). A nodal "eccentricity" option was used. The neutral axes of the beam elements were specified as offsets to the nodes at the slab nodes. The eccentricity provided for the required composite action between the beams and the concrete deck slab. The two-dimensional slab was modeled using plate elements and the composite beams were modeled using one-dimensional beam elements. The five transverse floor beams, as well as the two longitudinal girders, were modeled as non-prismatic members. Their section properties were calculated and input manually. The nodes for the slab plate elements had five degrees of freedom, and the beam elements had all six degrees of freedom.

RESULTS

It is assumed that the angles and bolts are failing due to the rotation of the longitudinal girder. This is causing a lateral differential displacement of the girder's top flange with respect to the concrete slab. Figure 4.2 shows the finite element model influence line for rotation of the longitudinal girder at the gaged abutment, quarter and center line points. It shows this line with a 75 kip load, incremented across the deck in the outside travel lane. This load was used to approximately represent an HS20 vehicle (72 kips) with impact and distribution. Figure 4.3 shows the field stress data in the same respective angle connection locations. Both figures show the abutment and quarter point rotations first increase at the same rate. They also show how the quarter point peaks at the midpoint of the graph, while the abutment peaks at the third point with a larger decreasing slope.

Additional collaboration is shown by the center line bolt. Although no strain gages were installed on the center line connection angle, a gaged bolt was installed in the center line's

lower bolt row. Figure 4.4 shows the stress in the center line bolt. This behavior indicates a stress reversal as the bolt goes from compression to tension, at approximately the midpoint of the truck loading event. This also corresponds to the rotational influence line for the center line point. All three graphs agree in rotational, out-of-plane displacement induced stress behavior at the abutment, quarter and center line connection points.

LOCAL CONNECTION MODEL

To study the influence of this deformation on the connection angle, a finite element plate model, with rectangular and triangular plate bending elements, was developed. The elements have three degrees of freedom per node. (See Figure 4.5.) Since the assumed behavior was that of a fixed-fixed column receiving a lateral displacement, the level at the upper row of bolts was modeled as a fixed support. The lower row of bolts was specified as a support in the areas surrounding the bolt's washer locations. The angle base, the bottom edge of the model, was specified as a fixed support that was assigned a lateral displacement.

Figure 4.6 shows the stress contours. The line of zero bending stress (inflection point) between the angle base and the lower bolt row. This corresponds with the assumed behavior of a fixed-fixed column with an induced lateral displacement as shown in Figure 2.8.

The effective bending stress range measured in the field, at the strain gage location, on the abutment angle is 12.85 ksi. It was determined that an out-of-plane displacement of 0.00248" at the abutment angle base is required to cause a 12.56 ksi bending stress at the gage location. This 12.56 ksi stress agrees with the calculated effective stress range of 12.85 ksi from the field data.

Since the rotation of the longitudinal girder will not substantially decrease with a stiffer angle, this lateral displacement will continue to occur for most reasonable angle thicknesses. For an infinite fatigue life, the maximum angle bending stress range is 8.8 ksi for this fatigue category. Table 4.1 shows how a change in the abutment angle's thickness would affect the bending stress at the base of the angle.

With a stiffer member, more moment and thus more stress is absorbed at that location in an indeterminate structure. Thus, it appears that cracking can not be prevented using available angle thicknesses.

	ABUTMENT ANGLE THICKNESS	STRESS AT ANGLE BASE
	3/4"	53.3 KSI
Existing Thickness:	**1/2"**	**26.7 KSI**
	1/4"	13.3 KSI

TABLE 4.1

ABUTMENT ANGLE THICKNESS vs BENDING STRESS

SUMMARY OF PROBLEM

The strain gage stress data show that the longitudinal girder's neutral axis lies above its center line. Therefore, partial composite action is occurring between the longitudinal girder and the concrete slab. The angle connections are, thus, acting as shear connectors. This was not an anticipated design behavior.

The rotational influence lines from the global finite element model correspond well with the field data bending stress patterns for the abutment, quarter point and center line angle locations. The angles and bolts are failing in fatigue due to the relative deformation of the top flange of the longitudinal girder with respect to the concrete slab when subjected to live loadings. This noncompatible, out-of-plane displacement induces large secondary bending stresses in the lower portion of the connection angle and prying forces on the lower bolt row. These secondary bending stresses are up to thirty times the corresponding bending stress of the longitudinal girder. The largest rotation and, thus, the largest number of failures occurs at the abutment locations. At the center line, where the rotation is the least, no bolt or angle failures have occurred.

Vibrational secondary bending stresses are also applied to the connection angle due to unsymmetrical loadings. This was demonstrated with the discussion of Figure 2.13. This was not anticipated during the design of these types of bridges. As a result, the heavy vehicles, traveling in either direction along this bridge, will cause either a high bending stress or a stress reversal on the abutment and quarter point connection angles. These angles are thus receiving many more bending stress applications and reversals than assumed in the original design.

CHAPTER 5

RECOMMENDATIONS

According to the results of this investigation, it is recommended that the top flange of the longitudinal girder not be connected to the transverse beam at the abutment and quarter point. This is confirmed by Fisher in studies of similar bridges (Fisher: 1977, 1978, 1984). This alteration will allow the deformation to occur. Currently, the fatigue prone angles and/or bolts will fail, allowing the required deformation to occur. This deformation may cause a crack to form in the transverse beam's web connection to the longitudinal girder (see Figure 2.3). This crack may be arrested with a hole drilled at the tip of the crack. Similarly, as Dr. Fisher has concluded for the Lehigh Canal Bridge, the failure of the Putnam Bridge connection will not impair the structural soundness of the Bridge. The center line connection should remain, since its effective stress range is well below that required for an infinite fatigue life. Also, the top (compression) flange of the longitudinal girder requires the lateral support provided by this connection to the transverse beam.

If truly desired, or later deemed necessary, a non-standard thickness 8"x4"x1/4" angle should replace the failing angles. The stress range will be approximately 13.3 ksi as shown in Table 4.1. This will allow for a 15 year life span based on the AASHTO Finite Life formula. Additionally, by not completely tightening the bottom row of bolts, an increase in the effective length used in the fixed-fixed column analogy will occur. This also would decrease the effective stress range and extend the service life of the connection angles and bolts.

REFERENCES

1. Dunker, K.F. and Rabbat, B.G., "Performance of Highway Bridges," Concrete International, Vol. 12, No. 8, August 1990, pp. 40-42.

2. "Guide Specifications for Fatigue Evaluation of Existing Steel Bridges," The American Association of State Highway and Transportation Officials, 1990.

3. "Standard Specifications for Highway Bridges," 14th edition, The American Association of State Highway and Transportation Officials, Washington, DC, 1989.

4. Fisher, J.W., Yen, B.T. and Daniels, J.H., "Fatigue Damage in the Lehigh Canal Bridge from Displacement-Induced Secondary Stresses," Fritz Engineering Laboratory, Lehigh University, November 1974.

5. Kulak, G.L., Fisher, J.W. and Struik, J.H., "Guide to Design Criteria for Bolted and Riveted Joints," 2nd Edition, John Wiley and Sons, New York, 1987, pp. 20.

6. Jategaonkar, R., Jaeger, L.G. and Cheung, M.S., "Bridge Analysis Using Finite Elements," Canadian Society for Civil Engineering, 1985, pp. 1-18.

7. "Proposed Revisions to the AASHTO Standard Specifications for Structural Supports for Highway Signs, Luminaries, and Traffic Signals," Section 1.9.6 - Vibration and Fatigue.

8. Fisher, J.W., "Bridge Fatigue Guide: Design and Details," American Institute of Steel Construction, New York, 1977, pp. 39-40.

9. Fisher, J.W., "Fatigue and Fracture in Steel Bridges," John Wiley and Sons, New York, 1984.

10. Fisher, J.W., "Fatigue Cracking in Bridges from Out-Of-Plane Displacements," Canadian Journal of Civil Engineering, Vol. 5, 1978, pp. 553-555.

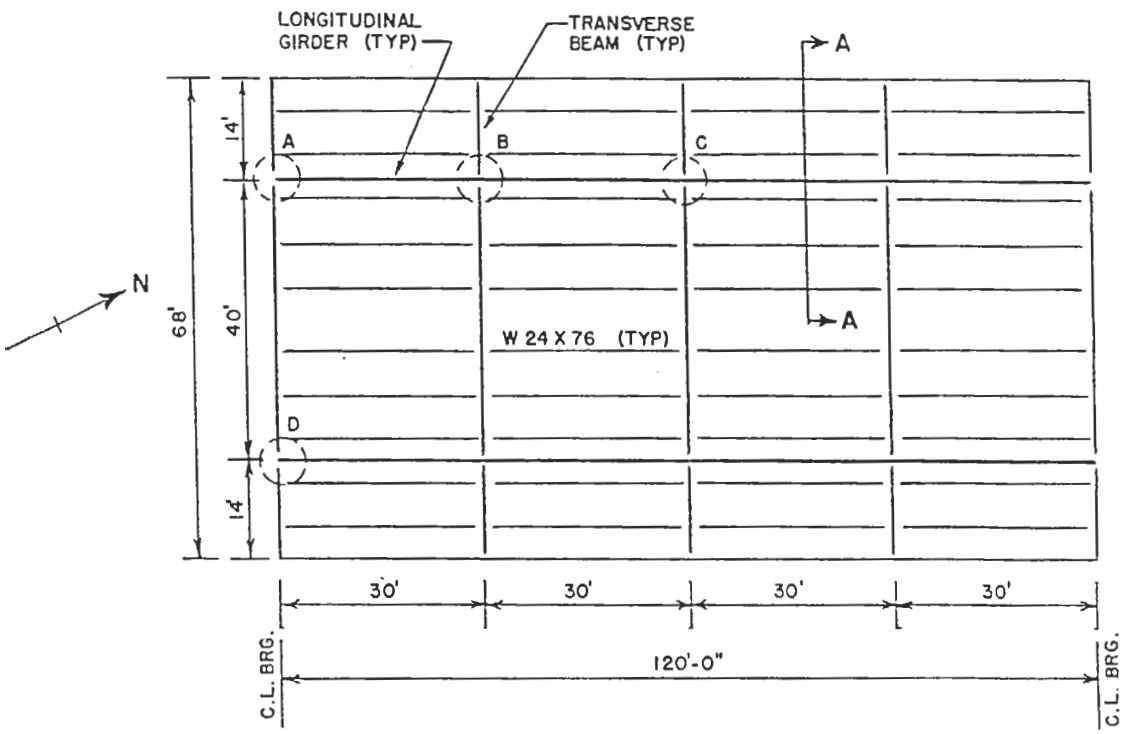

Figure 2.1 Plan View of Test Span

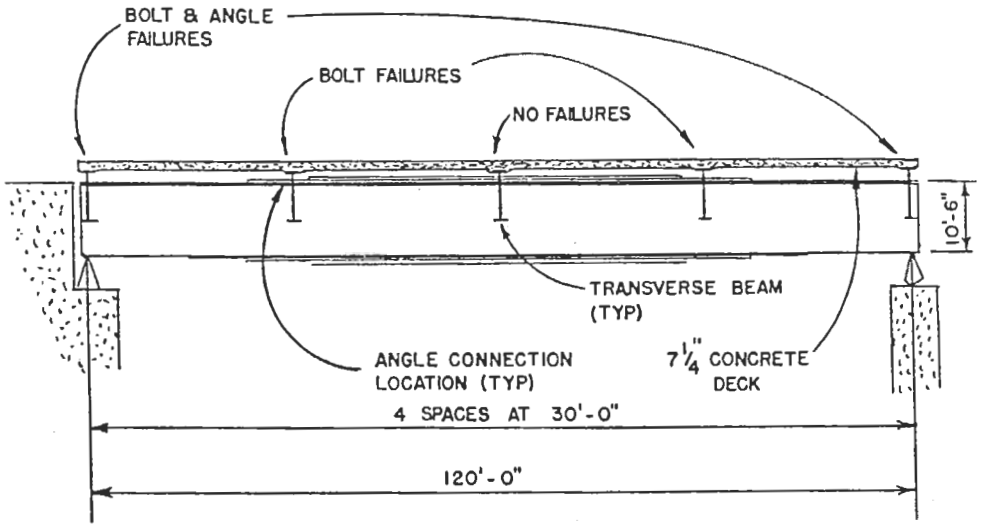

Figure 2.2 Elevation of Test Span

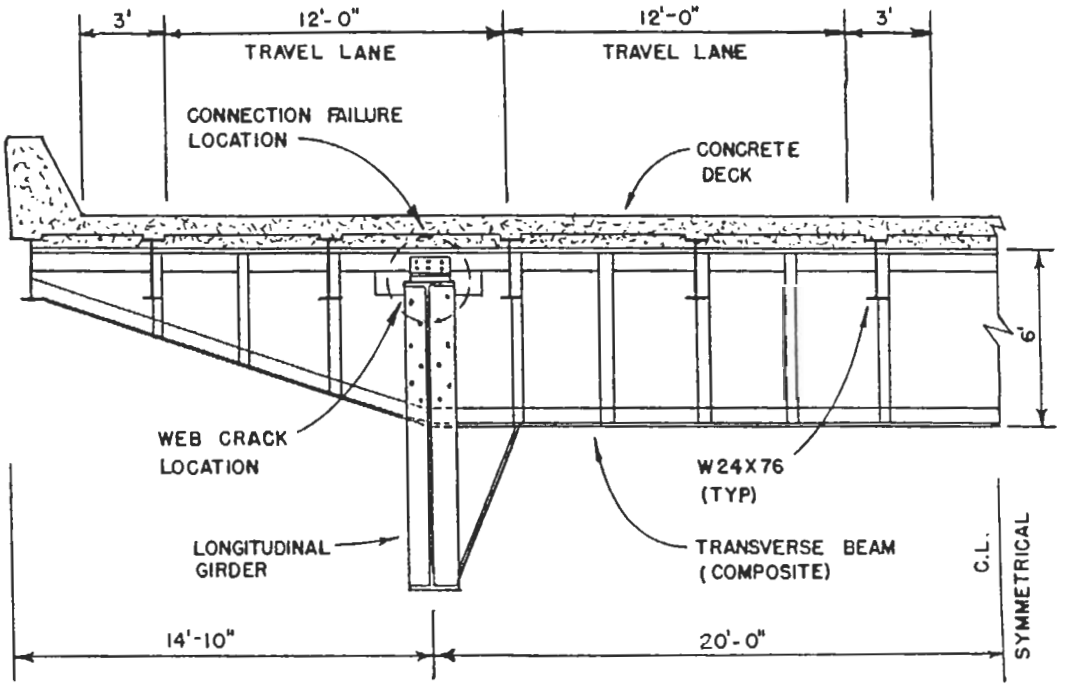

Figure 2.3 Transverse Section A-A

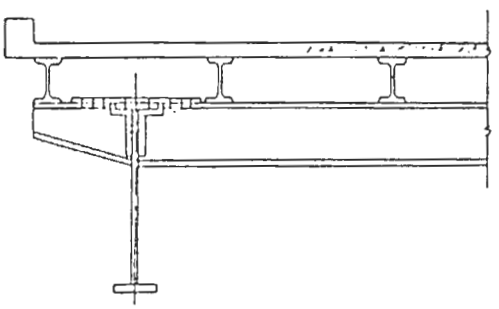

Figure 2.4 Transverse Cross Section of Lehigh Canal Bridge

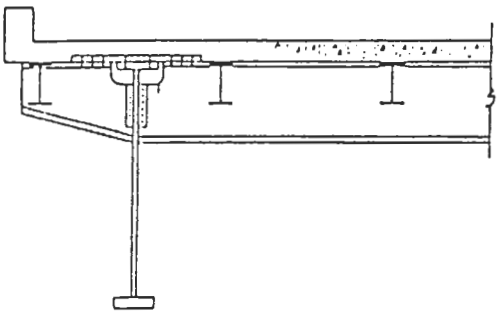

Figure 2.5 Transverse Cross Section of Improved Design

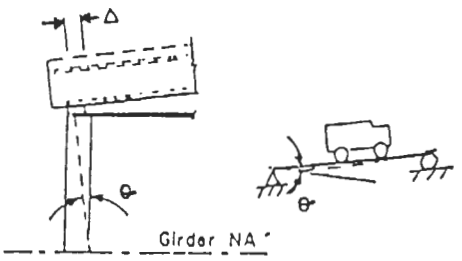

Figure 2.6 Schematic of Deformation Induced into Connection Angle

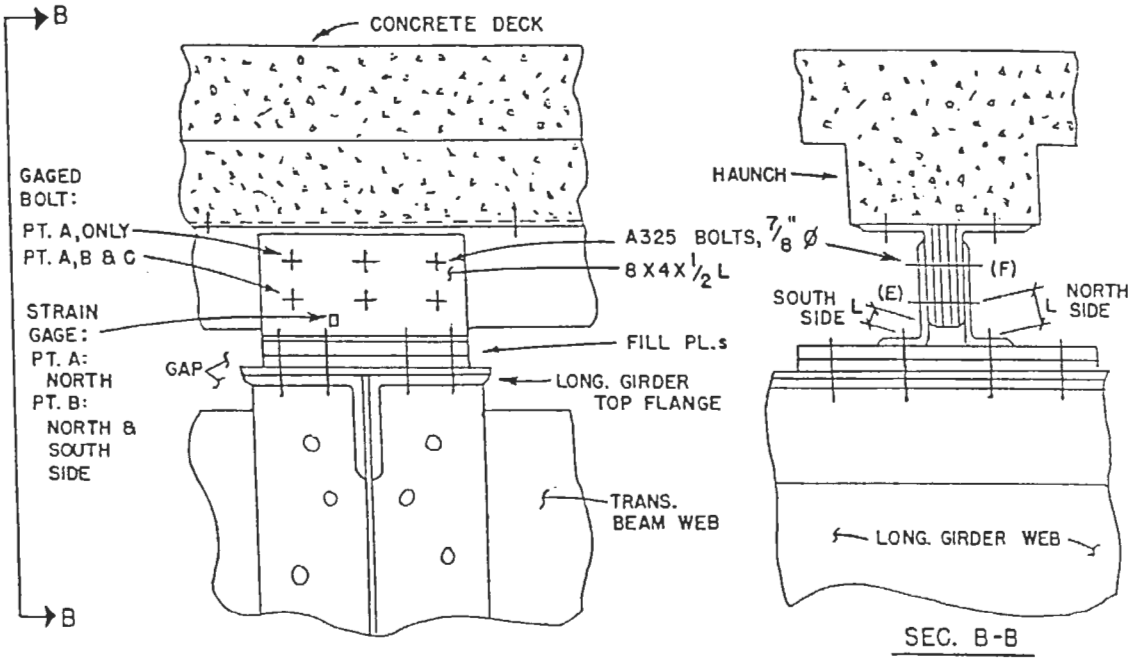

Figure 2.7 Detail and Section B-B of Connection

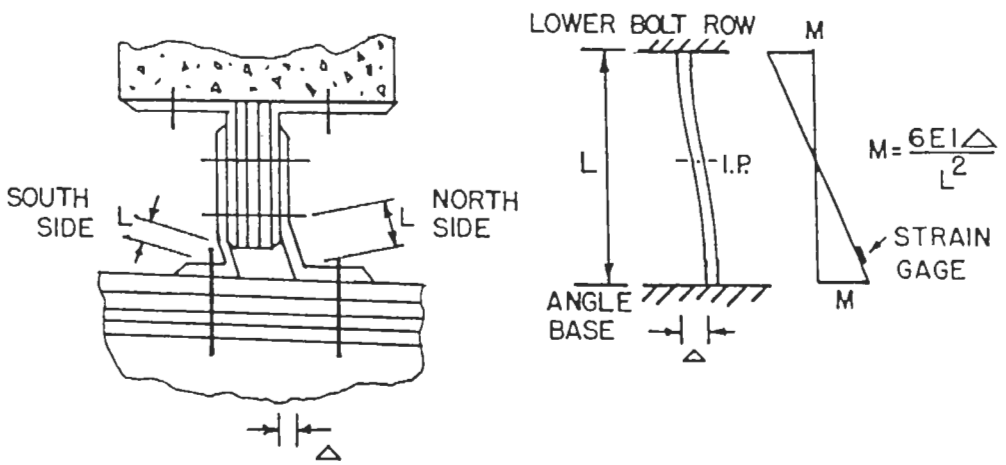

Figure 2.8 Fixed-Fixed Column Analogy

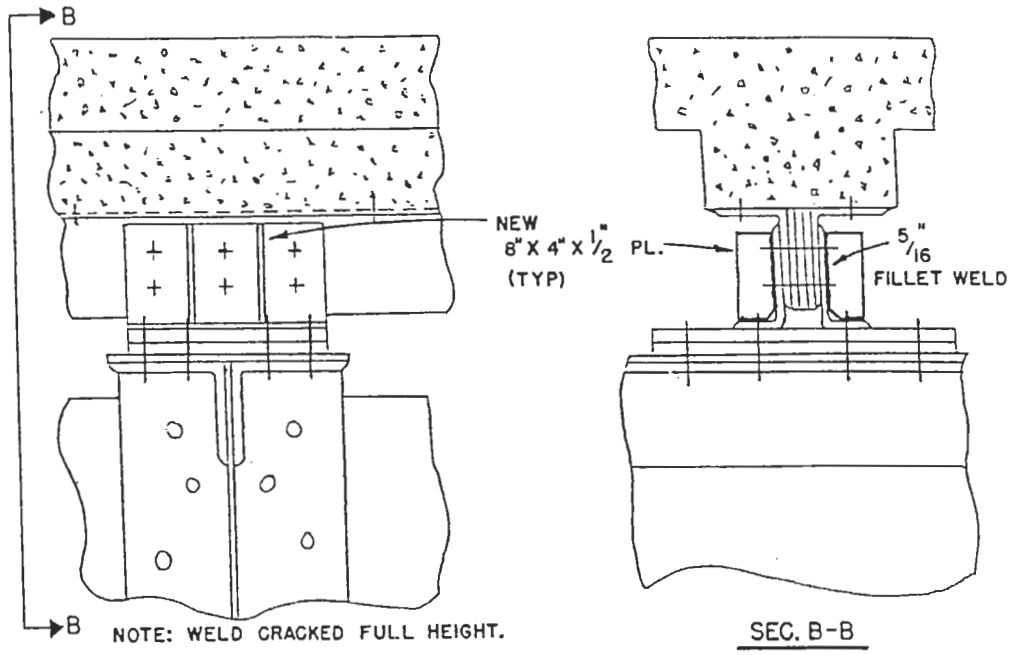

Figure 2.9 Details of Connection Modification

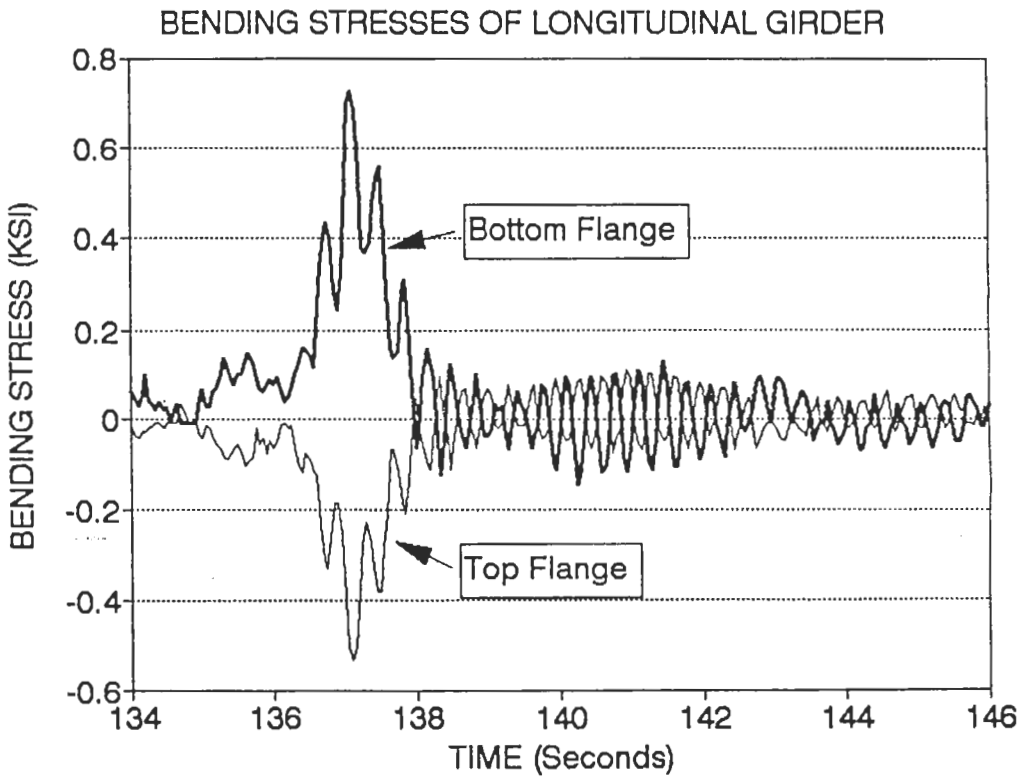

Figure 2.10 Top and Bottom Longitudinal Girder Center Line Bending Stresses

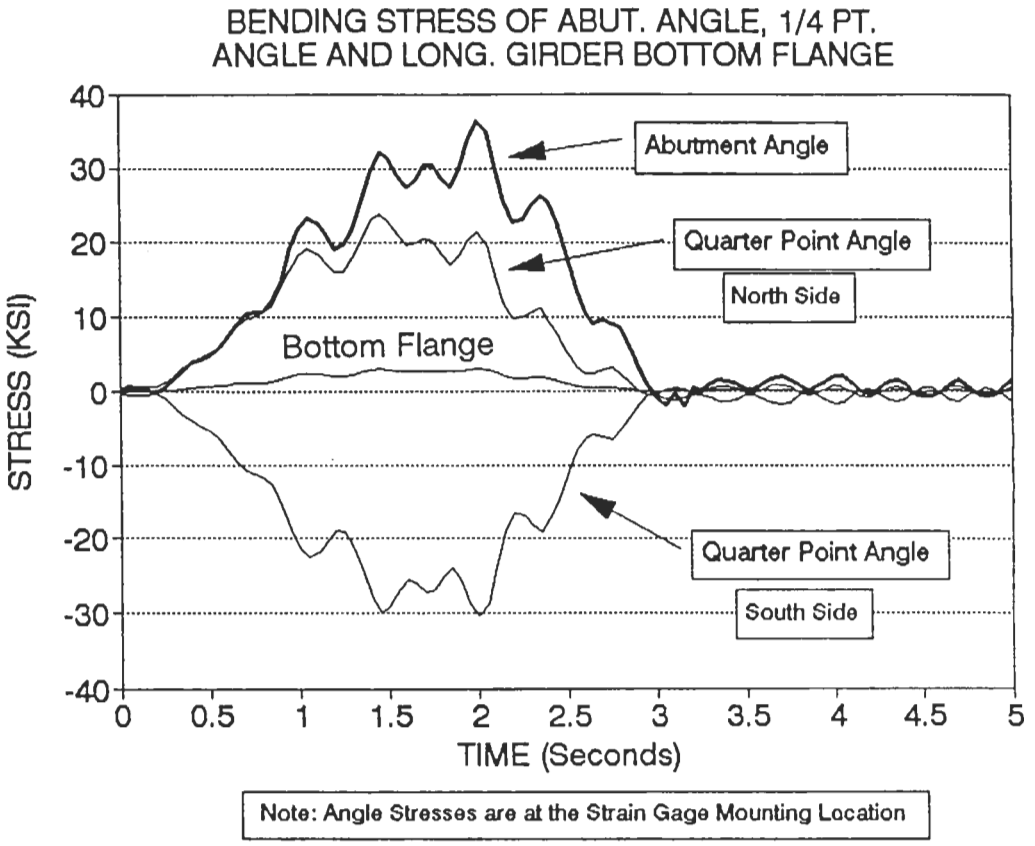

Figure 2.11 Maximum Stresses Recorded at Angles and Girder Flange

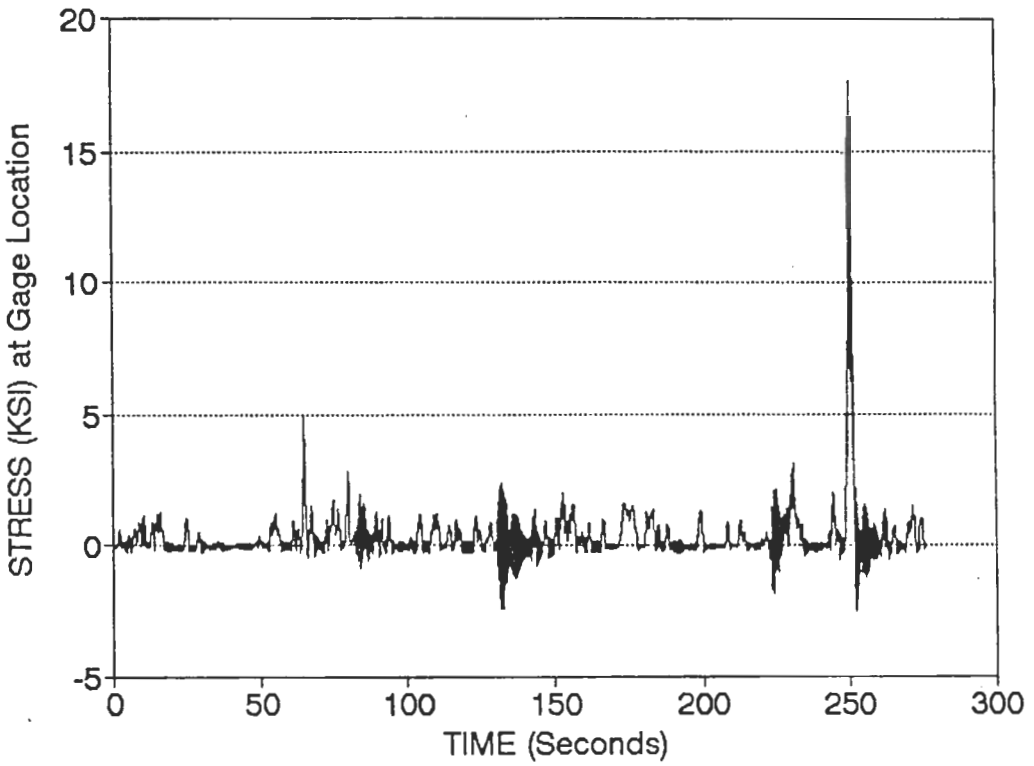

Figure 2.12 Typical Strain Gage Data at Abutment Angle

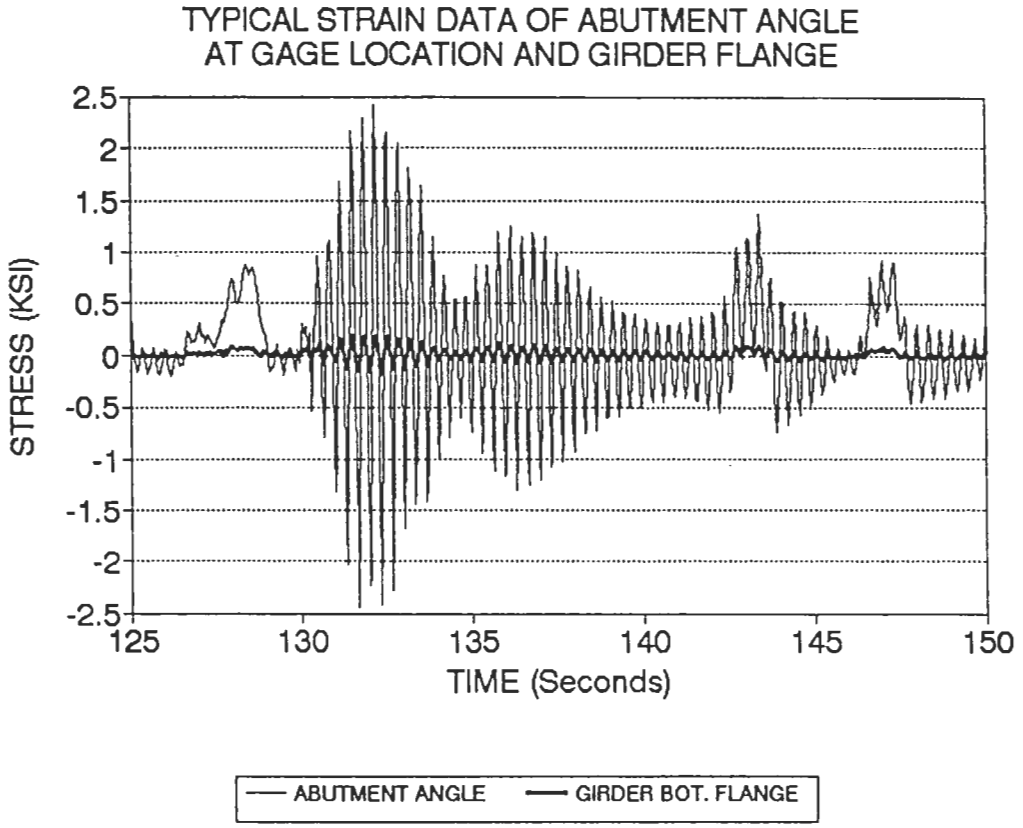

Figure 2.13 Detail of Fig. 2.13 at a Specific Time Interval

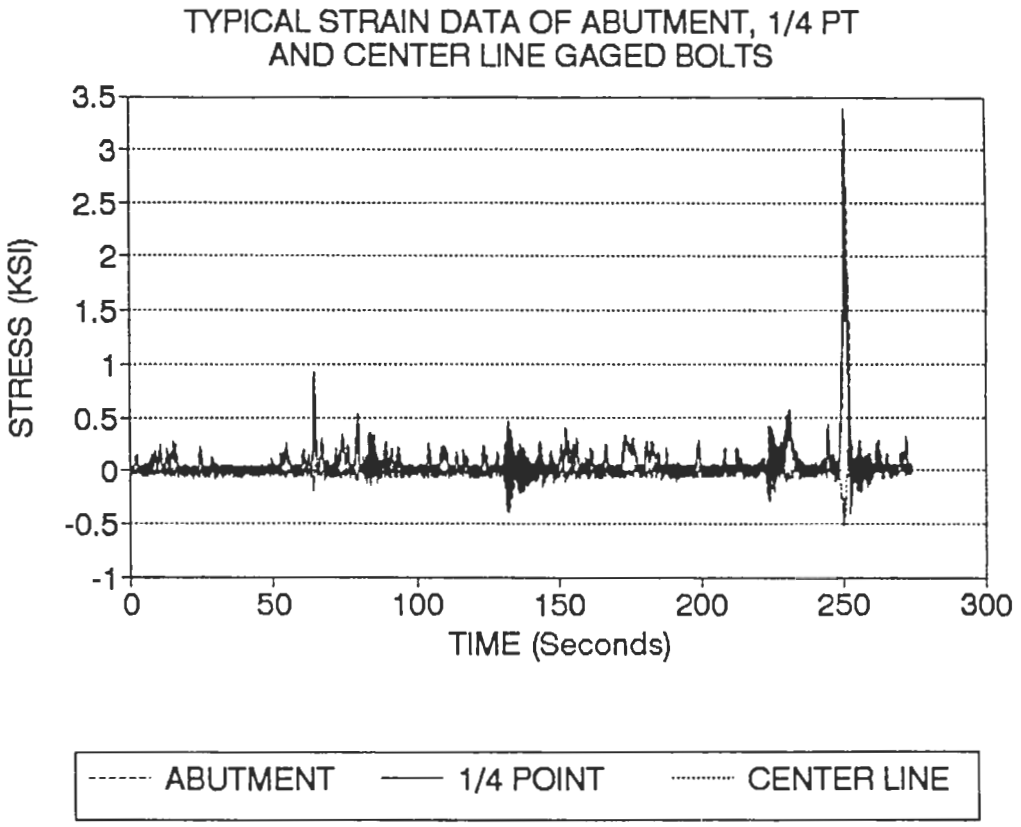

Figure 3.1 Typical Bolt Stress Data at the Abutment, Quarter Point and Center Line Connections

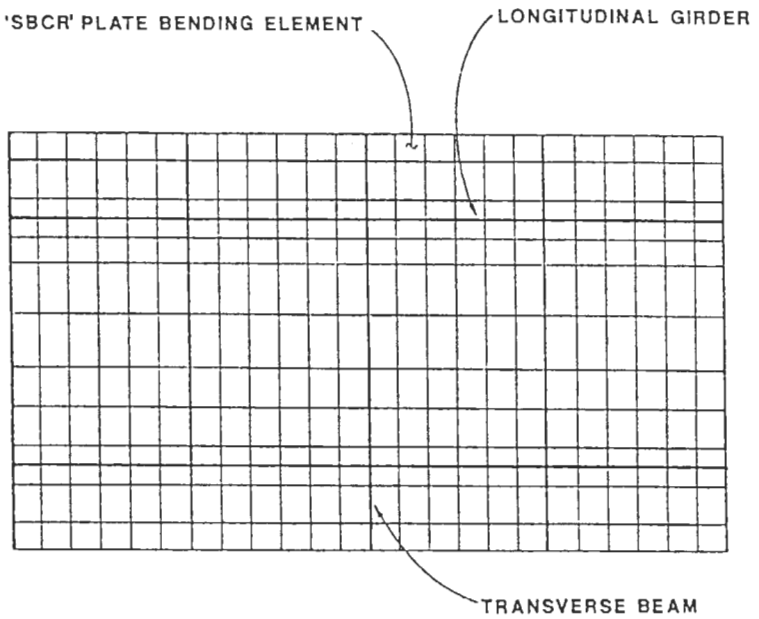

Figure 4.1 Global Finite Element Model of Test Span

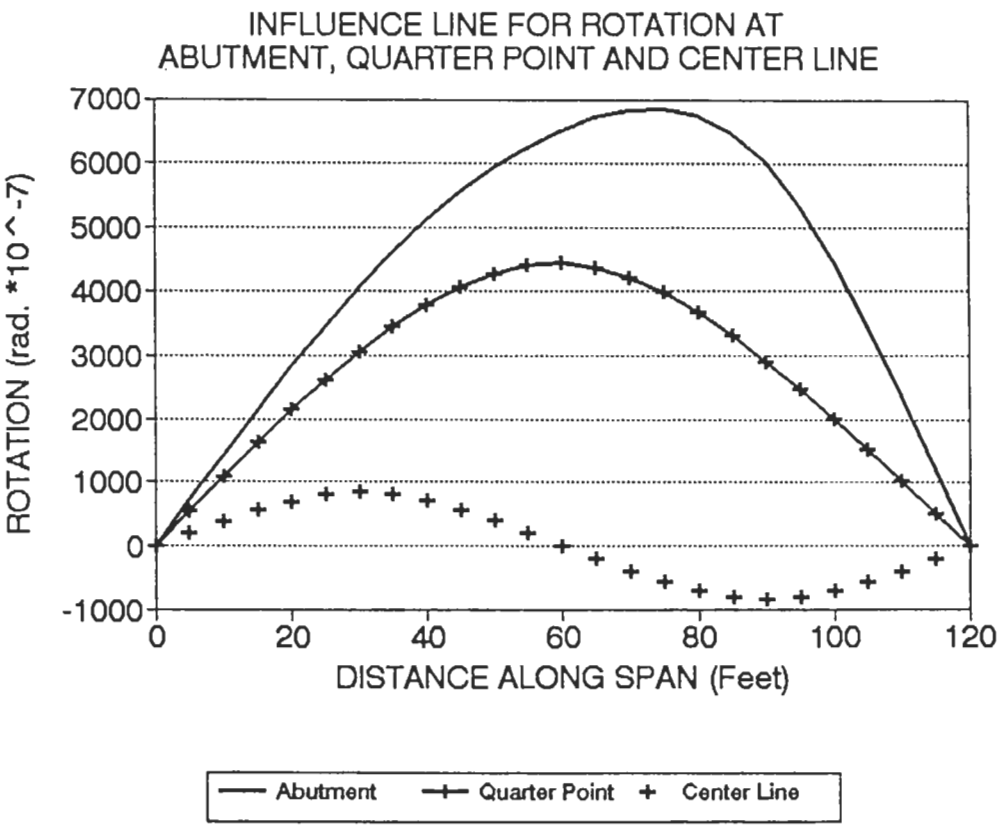

Figure 4.2 Rotational Influence Line for Angle Locations

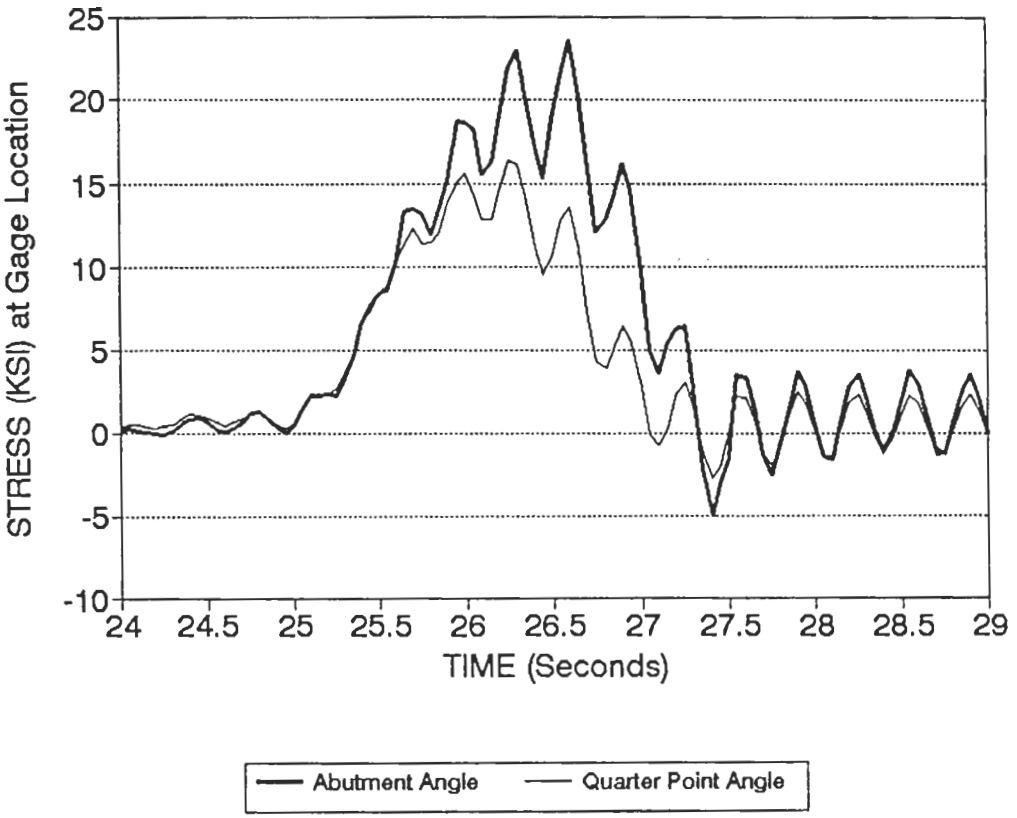

Figure 4.3 Stress Loading Behavior of Abutment and Quarter Point Connection Angles

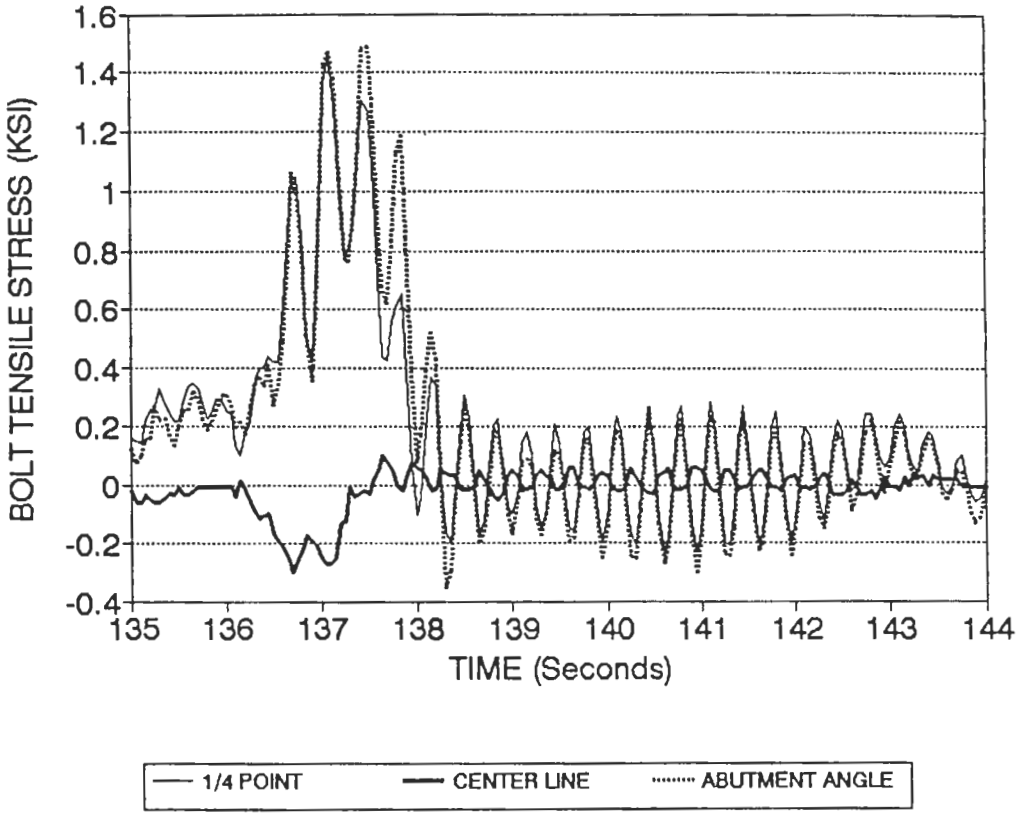

Figure 4.4 Center Line Bolt Displaying a Stress Reversal

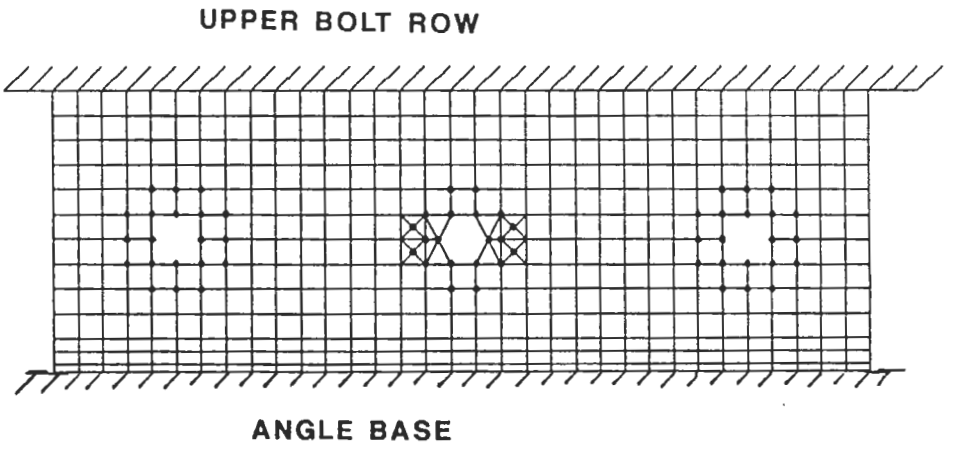

Figure 4.5 Local Finite Element Model of Connection Angle

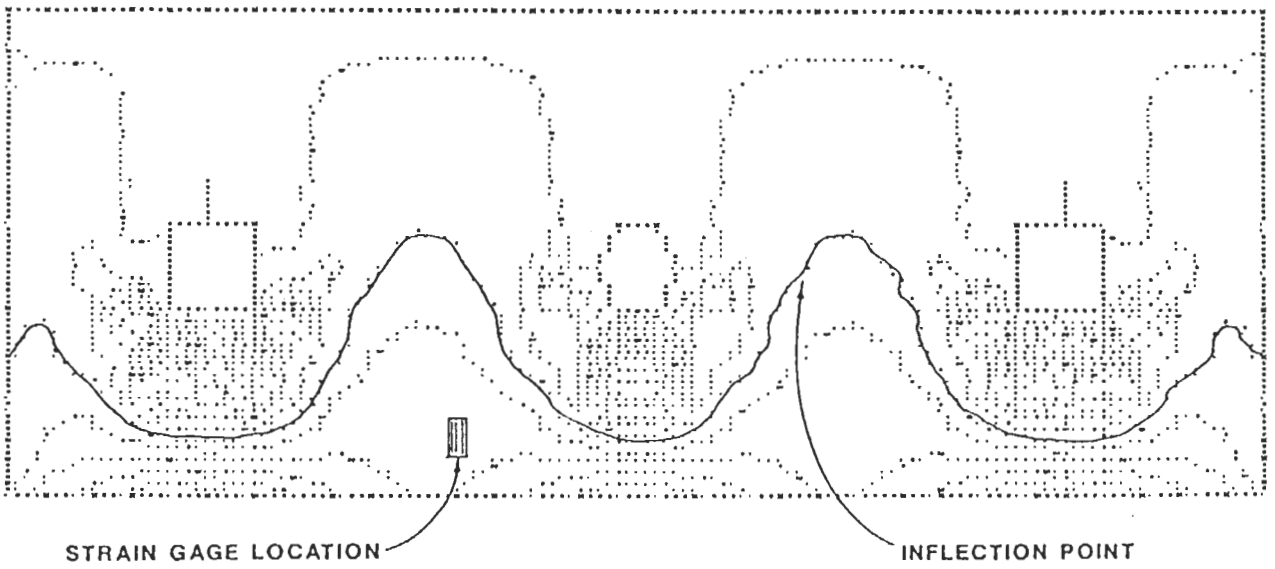

Figure 4.6 Bending Stress Distribution of Local Finite Element Model